robotics

MDPI

Article

The Impact of Kinematic Redundancy on the Energetic Performance of Robotic Manipulators †

Giuliano Fabris, Lorenzo Scalera * and Alessandro Gasparetto

Polytechnic Department of Engineering and Architecture, University of Udine, 33100 Udine, Italy; giuliano.fabris@uniud.it (G.F.); alessandro.gasparetto@uniud.it (A.G.)

* Correspondence: lorenzo.scalera@uniud.it

† This paper is an extended version of our paper published in: Fabris, G.; Scalera, L.; Gasparetto, A. Leveraging Kinematic Redundancy for Energy Efficiency in a 8-DOF Robotic System. In: Carbone, G., Quaglia, G. (Eds.) Proceedings of I4SDG Workshop 2025—IFToMM for Sustainable Development Goals. I4SDG 2025. Mechanisms and Machine Science; Springer: Cham, Switzerland, 2025; Volume 179, pp. 340–348.

Abstract

Energy efficiency is a challenging research topic in robotics, since it can reduce operating costs and increase production sustainability. In this paper, we present a strategy for energy-efficient trajectory planning in redundant robotic systems. The proposed approach aims at optimizing the solution of inverse kinematics at each of the waypoints that define the considered task, so as to minimize the energy consumption. The approach is validated with simulations and bespoke experiments on two different robotic systems with seven and eight degrees of freedom (DOFs). Two test cases are considered, i.e., a point-to-point motion and a pick-and-place task. The experimental results quantify the energy saving capabilities of the proposed approach up to 82.54% and 94.28% with the seven-DOF and eight-DOF robots, respectively, with respect to reference cases.

Keywords: energy efficiency; kinematic redundancy; motion planning; optimization; robotics; sustainability

1. Introduction

In recent years, the industrial sector has experienced a steady increase in the deployment of robotic systems, since robots can support or replace human operators in dangerous and repetitive tasks, while increasing productivity and process quality [1]. Nevertheless, this trend has resulted in a growth in the overall energy demand [2]. As a consequence, improving energy efficiency in robotics has become a key factor for the sustainable development of modern industry [3,4]. This need is also emphasized by the Sustainable Development Goals (SDGs) of the United Nations [5], as in the SDG9 (Industry, Innovation, and Infrastructure), and in the SDG12 (Responsible Consumption and Production).

The reduction in energy consumption in robotic systems can be achieved through several strategies. These include the design and optimization of the robot's physical structure [6], the integration of energy-efficient components such as regenerative drives [7], as well as the optimization of the configuration of modular robots [8]. Furthermore, alternative approaches to minimize the energy expenditure are the optimization and exploitation of joint elastic properties [9,10], the optimal positioning of the task within the robot workspace [11,12], the optimization of the execution time [13,14], and motion law parameters [15–17].

Academic Editor: Raffaele Di Gregorio

Received: 22 January 2026
Revised: 21 February 2026
Accepted: 25 February 2026
Published: 27 February 2026

When dealing with redundant robotic systems, leveraging kinematic redundancy could be a further strategy to achieve energy efficiency. A robotic system is considered kinematically redundant when its number N of degrees of freedom (DOFs) exceeds the number R of operational space variables required to describe a pre-defined task [18]. Redundancy increases the flexibility of redundant robots with respect to non-redundant ones, since it can be exploited to fulfill a secondary task (e.g., collision avoidance, manipulability maximization, or energy efficiency), without altering the motion of the end-effector during the execution of the desired primary operation [19]. In the literature, a wide range of redundancy resolution approaches has been investigated. For example, the solution to the inverse kinematics problem can be obtained with the purpose of avoiding collisions and singularities and maximizing manipulability. In this context, Monari et al. present an approach that relies on null space projection to avoid collisions [20]. Differently, the authors in [21] propose avoiding self-collisions by adding an interference vector, obtained from reinforcement learning, to the joint velocities in the computation of the pseudo-inverse of the Jacobian matrix. The authors in [22] consider null space projection for avoiding singularities, solving the inverse kinematics problem locally. Moreover, Vu et al. present an approach for finding the solution of the inverse kinematics that maximizes the manipulability thanks to an artificial neural network [23]. Nguyen et al. achieve several secondary tasks, i.e., collision avoidance, manipulability maximization, and singularity avoidance through null space projection [24]. Kinematic redundancy can also be exploited for respecting joint limits. An example is the Saturation in the Null Space (SNS) approach [25,26], which considers joint limits as hard constraints. That approach adopts null space projection and a task-scaling strategy for redistributing the joints motion in order to ensure task feasibility.

Energy efficiency is another secondary task that can be fulfilled through optimal redundancy resolution. Doan et al. propose to minimize the consumed energy during a welding operation by optimizing the end-effector torch angle with a modified particle swarm optimization scheme, also avoiding collisions and joint limits [27]. Ruiz et al. consider motion predictive control for finding the energy-optimal position of the redundant joints in a planar parallel robot, keeping it steady during motion [28]. Furthermore, the authors in [29] propose reducing the energy expenditure through the optimization of the Cartesian inertia of the robot, whereas Li et al. propose an energy-optimal redundancy resolution approach combining deep reinforcement learning and an artificial neural network [30].

Differently from previous approaches, in this paper we present a strategy for energy-efficient trajectory planning in redundant robotic systems, based on the optimization of the position of selected redundant joints at each of the waypoints that define the task to be executed, given the total execution time. In this manner, the solution of the inverse kinematics is not left to chance, but it is selected through an optimization procedure that aims at maximizing the energetic performance of the system. The proposed approach is validated on two different robotic systems, i.e., a seven-DOF robotic manipulator and eight-DOF robot (composed of a seven-DOF arm mounted on a linear axis). A point-to-point motion and a pick-and-place task are adopted as test cases. The results of extensive numerical simulations and experimental tests allow us to quantify the actual savings of the proposed approach, and demonstrate its capability to reduce energy consumption with respect to reference trajectories. The experimental results highlight a percentage reduction of energy consumption up to 82.54% with the seven-DOF arm, and up to 94.28% with the eight-DOF robot.

This work is an extended version of our previous conference paper in [31]. With respect to [31], the following improvements are implemented here: (i) the evaluation of the performance of the proposed approach considering two robotic systems with a different degree of redundancy, to demonstrate the modularity and scalability of our strategy;

(ii) the comparison with the Saturation in the Null Space approach in [25]; (iii) the results of an extensive experimental validation of the proposed approach, assessing the energy consumption reduction with respect to reference trajectories.

The paper is organized as follows: Section 2 describes the proposed approach for achieving energy efficiency in redundant robotic systems. Section 3 illustrates the considered case studies. Section 4 reports the numerical results and the comparison with the SNS approach, whereas the experimental validation of the proposed approach is illustrated in Section 5. Finally, Section 6 concludes the work.

2. Kinematic Redundancy for Energy Efficiency

In this paper, an approach for minimizing the energy consumption of redundant robotic systems is proposed. The strategy exploits kinematic redundancy to optimize the solution of the inverse kinematic problem and define an energy-optimal trajectory of the robot. The proposed approach takes as inputs a sequence of waypoints defined in the 3D space as positions and orientations that the end-effector of the robot has to reach during its motion, and the time distances between each pair of consecutive waypoints (with a total execution time T). Before the optimization, a number of joints equal to the degree of redundancy ($N - R$) of the considered robotic system is considered. Then, the proposed strategy aims at optimizing the position $\boldsymbol{q}^*$ of the selected set of redundant joints for each waypoint. In this way, the positions of the redundant joints $\boldsymbol{q}^*$ are considered as optimization variables, enabling the algorithm to obtain the optimal solution of the inverse kinematic problem at each waypoint by adjusting the robot configuration, without altering the desired end-effector pose. Once the joint configuration is defined for each waypoint, the joint-space trajectory $(\boldsymbol{q}, \dot{\boldsymbol{q}}, \ddot{\boldsymbol{q}})$ is derived through interpolation between the waypoints.

The joint torques required to drive the robot along the desired trajectory can be computed as:

$$\boldsymbol{\tau} = \boldsymbol{M}(\boldsymbol{q})\ddot{\boldsymbol{q}} + \boldsymbol{C}(\boldsymbol{q}, \dot{\boldsymbol{q}})\dot{\boldsymbol{q}} + \boldsymbol{g}(\boldsymbol{q}) + \boldsymbol{F}_f \tag{1}$$

where $\boldsymbol{M}(\boldsymbol{q})$ is the mass matrix and $\boldsymbol{C}(\boldsymbol{q}, \dot{\boldsymbol{q}})$ accounts for the Coriolis and centrifugal effects, whereas $\boldsymbol{g}(\boldsymbol{q})$ represents the gravitational term. Furthermore, $\boldsymbol{F}_f$ takes the friction effects into account. The optimization problem presented in this work is formulated as:

$$\min_{\boldsymbol{q}*} \; E \quad \text{where} \quad E = \sum_{i=1}^{N} \int_0^T P_i \, dt \tag{2}$$

where P_i represents the mechanical power of the i-th joint of the N-DOF robot computed from the absolute values of the corresponding joint torque and joint velocity. E accounts for the total mechanical energy required by the robot to execute the desired motion, including the energy needed during both the acceleration and deceleration phases. In this work, regenerative effects and energy recovery during braking phases are not considered. This choice is motivated by the fact that the majority of industrial robots are not equipped with power regeneration systems and, therefore, cannot recover braking energy, which is instead dissipated as heat on a resistor.

The optimization problem in Equation (2) is subject to the following constraints:

$$\begin{cases} q_{min} < q < q_{max} & q_{min}, q_{max} \text{ lower and upper joint position limits} \\ |\dot{q}| < \dot{q}_{max} & \dot{q}_{max} \text{ joint velocity limit} \\ |\ddot{q}| < \ddot{q}_{max} & \ddot{q}_{max} \text{ joint acceleration limit} \\ |\dddot{q}| < \dddot{q}_{max} & \dddot{q}_{max} \text{ joint jerk limit} \\ |\tau| < \tau_{max} & \tau_{max} \text{ joint torque limit} \\ |\dot{p}| < \dot{p}_{max} & \dot{p}_{max} \text{ end-effector velocity limit} \\ |\ddot{p}| < \ddot{p}_{max} & \ddot{p}_{max} \text{ end-effector acceleration limit} \\ |\dddot{p}| < \dddot{p}_{max} & \dddot{p}_{max} \text{ end-effector jerk limit} \end{cases} \quad (3)$$

This paper focuses on mechanical energy, which is directly determined by the robot trajectories and thus represents a relevant measure for evaluating the effectiveness of the proposed optimization strategy in terms of energy expenditure. The robotic system is modeled as an open kinematic chain of rigid bodies, and the joints are considered to be ideal without clearance. The proposed approach assumes that the robot nominal kinematics and dynamics parameters, along with its kinematics and dynamics limits, are known. Moreover, this work does not account for uncertainty in the robot dynamics parameters.

3. Case Studies

In this section, we first describe the two redundant robotic systems considered in this work. Then, the trajectories designed for evaluating the performance of the proposed approach are presented.

3.1. 7-DOF Robot

In the first case study, we consider a Panda arm by Franka Robotics GmbH (Munich, Germany) with seven degrees of freedom (Figure 1). The robot has an operational reach equal to 855 mm, a pose repeatability of ±0.1 mm, and a payload of 3 kg. The joint torques and the consumed mechanical energy are computed as in Equation (1), considering the dynamic model of the Panda arm identified in [32]. The model in [32] describes friction forces as a sigmoidal function that also accounts for friction torques at low joint velocities. In the considered test case, the robot executes the prescribed trajectories with no payload applied to its end-effector.

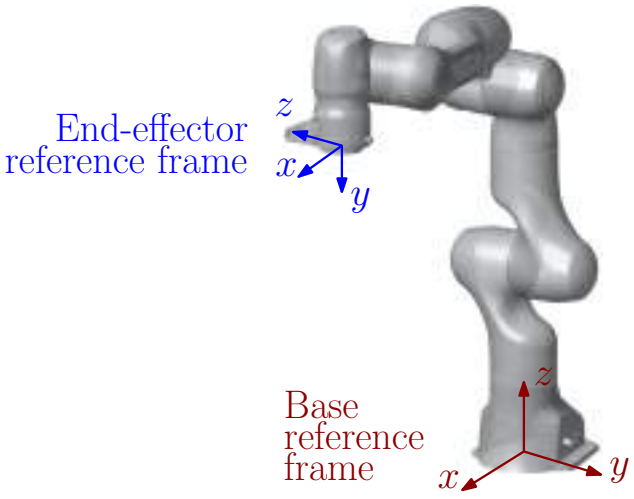

Figure 1. Representation of the 7-DOF robot considered in the first test case.

If a six-dimensional task is considered, the degree of redundancy of the arm is equal to $N - R = 1$. In this case, the position q^* of only one joint of the robot is selected for the

energy-efficient optimization at each path point. In different independent optimizations, all joints of the seven-DOF robot are considered as optimization variables, with the aim of determining which leads to the greatest energy saving with respect to a reference case.

Although the proposed approach selects a specific number of redundant joints and optimizes their positions at waypoints, the target of the optimization is the definition of an optimal robot configuration, which is the inverse kinematics solution based on those joint position values. Therefore, the selection of a specific joint (or set of joints) to be optimized influences the way of exploring the space of candidate solutions of the optimization problem (robot configurations) within the infinite space of possible solutions of the inverse kinematics. The joints that provide the largest energy savings are those that allow a better exploration of the solution space and help avoid potential local minima in the optimization. By optimizing these joints, the proposed strategy can more effectively adjust the robot configuration along the trajectory, leading to more significant reductions in mechanical energy. The choice of which joint to optimize is not absolute, as it depends on multiple factors, including the specific task to be executed, the desired trajectory, and the characteristics of the robotic system. Therefore, predicting the most effective joint for a given case is not straightforward and represents an interesting and challenging direction for future work.

3.2. 8-DOF Robot

In the second case study, we consider a robotic system composed of a Panda arm mounted on a linear axis, shown in Figure 2. The Panda arm is the same considered in the first test case, and its modeling approach is described in Section 3.1. As in the previous case, no payload is considered to be applied to the robot end-effector. The linear axis has a total length of 0.8 m and allows it to move the base of the arm using a cart driven by means of a pulley-belt system. The driven pulley is actuated by a brushless motor through a planetary gearbox. A graphical overview of the belt-driven linear axis is shown in Figure 3.

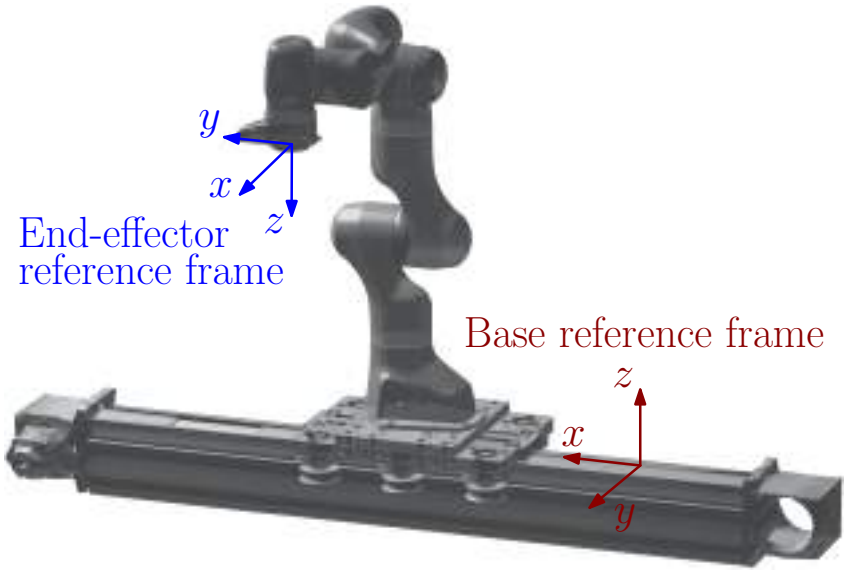

Figure 2. Representation of the 8-DOF robot considered in the second test case.

The total number of degrees of freedom of the robotic system is equal to 8. When considering a six-dimensional task, the degree of redundancy is equal to $N - R = 2$. Therefore, for each considered waypoint it is required to optimize the positions $\boldsymbol{q}^*$ of two redundant joints to find an energy-optimal solution of the inverse kinematics problem. Given that the positions $\boldsymbol{q}^*$ of two different redundant joints have to be optimized for each waypoint, in this second test case we evaluate all possible combinations of two different

joints to be optimized in order to find the one that minimizes the energy consumption. As in the first case study, determining a criterion for the selection of the pair of joints to be optimized is beyond the scope of this work. Compared to the first robotic arm, the increased degree of redundancy (and the resulting higher number of optimization variables) expands the possibilities of trajectory optimization. However, the eight-DOF robotic system includes one additional motor compared to the previous case, which can result in higher energy consumption.

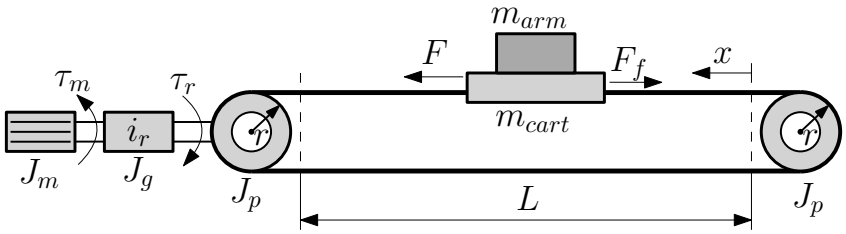

Figure 3. Model of the linear axis of the considered 8-DOF robot.

The dynamic parameters needed to compute the joint torques and the mechanical energy consumption of the linear axis are retrieved from [14]. The joint torque τ_0 of the linear axis required to execute the trajectory $(q_0, \dot{q}_0, \ddot{q}_0)$ can be obtained as

$$\tau_0 = r\left[\left(m + \frac{(J_m + J_g)\, {i_r}^2 + 2J_p}{r^2}\right)\ddot{q}_0 + a_1 \,\mathrm{sign}(\dot{q}_0) + a_2\,\dot{q}_0 + a_3 \,\mathrm{atan}(a_4\,\dot{q}_0)\right] \tag{4}$$

where $m = m_{cart} + m_{arm}$ denotes the sum of the masses of the cart and the robotic arm and i_r is the gear ratio. J_m, J_g, and J_p represent the inertia of the motor, gearbox, and pulleys, respectively. The parameter r represents the pulley radius, whereas a_1, a_2, a_3, and a_4 are the coefficients considered for modeling Coulomb (a_1 sign$(\dot{q}_0)$) and viscous friction ($a_2\,\dot{q}_0$), as well as low-speed friction effects (a_3 atan$(a_4\,\dot{q}_0)$). The values of these parameters used in the numerical optimizations are reported in Table 1.

Table 1. Geometrical and dynamical parameters of the linear axis.

Parameter	Symbol	Value	Parameter	Symbol	Value
Motor inertia	J_m	9.3×10^{-5} kg m^2	Pulley radius	r	0.045 m
Gearbox inertia	J_g	7.0×10^{-5} kg m^2	Axis length	L	0.8 m
Pulley inertia	J_p	2.1×10^{-3} kg m^2	Coulomb friction	a_1	0.0 N
Cart mass	m_{cart}	18.69 kg	Viscous friction	a_2	351.28 Ns/m
Arm mass	m_{arm}	17.80 kg	Low-speed friction	a_3	197.35 N
Gear ratio	i_r	10	Low-speed friction	a_4	159.43

3.3. Tested Trajectories

The performance of the proposed optimization approach is evaluated through two six-dimensional tasks defined in the 3D space. The first test case (named Test A) is a point-to-point motion defined by two waypoints, shown in Figure 4. The linear distance between the waypoints is equal to 1.0 m, and the movement has to be executed in a total time equal to T = 2.5 s. The trajectory is planned using a fifth-degree polynomial motion law in the joint space. The position of the waypoints of Test A for the two considered robotic systems with respect to their base reference frame are reported in Table 2. The base reference frames of the seven-DOF and the eight-DOF robots are shown in Figure 1 and Figure 2, respectively. The orientation of the end-effector is defined using angles φ, ϑ, and ψ and following the roll–pitch–yaw convention.

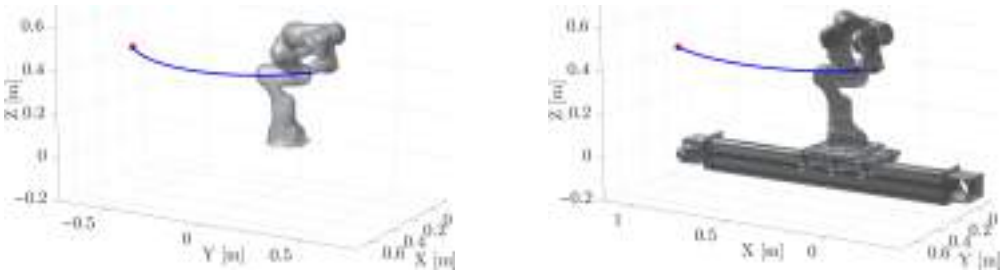

(**a**) (**b**)

Figure 4. 3D path of the reference case Test A for the 7-DOF robot (**a**), and for the 8-DOF robot (**b**).

Table 2. Desired pose of the end-effector of the two considered robotic systems for each of the waypoints of the trajectory in Test A.

Robot	Waypoint	x [m]	y [m]	z [m]	ψ [rad]	ϑ [rad]	φ [rad]
7-DOF robot	1	0.50	0.50	0.50	$11\pi/12$	$\pi/12$	$-\pi/4$
	2	0.50	-0.50	0.50	$13\pi/12$	$-\pi/12$	$-\pi/4$
8-DOF robot	1	-0.10	0.50	0.50	$11\pi/12$	$\pi/12$	$\pi/4$
	2	0.90	0.50	0.50	$13\pi/12$	$-\pi/12$	$\pi/4$

For the second test (Test B), we consider a pick-and-place task, composed of two vertical movements and one horizontal translation. The task is defined by four waypoints in the 3D space, as it can be seen in Figure 5. The vertical ascent and descent are 0.3 m long and have to be executed in 1.3 s each, whereas the horizontal movement has a length equal to 0.8 m and a duration of 2.4 s. The total execution time is equal to 5 s. Spline curves are adopted to plan the trajectories of the robots through the selected waypoints. More specifically, the considered spline algorithm uses fourth-degree polynomials for the initial and final segments of the motion, whereas third-degree polynomials are employed for the intermediate segments. The position of the waypoints of Test B for the two considered robotic systems with respect to their base reference frame are reported in Table 3.

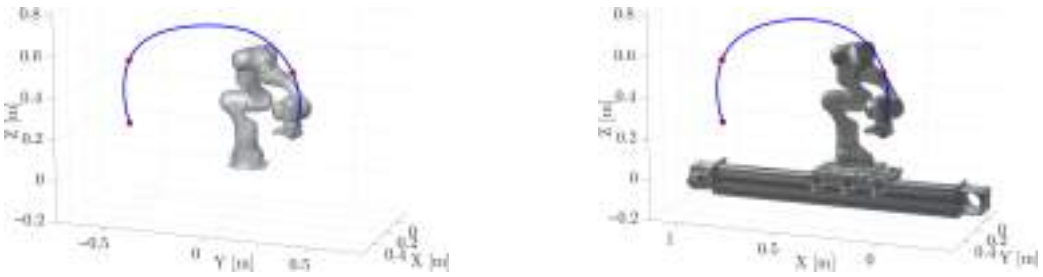

(**a**) (**b**)

Figure 5. 3D path of the reference case of Test B for the 7-DOF robot (**a**), and for the 8-DOF robot (**b**).

For each test and each case study, we define a reference case with respect to which the energy consumption reduction is computed. The reference cases are defined by selecting for each waypoint the solution of the inverse kinematics closest to a homing position. The joint positions in the homing configurations for both considered robotic systems are reported in Table 4. The joint q_0 represents the linear axis, whereas the joints from q_1 to q_7 are the joints of the Panda arm.

The optimization problem defined in Equation (2) with Equation (3) is implemented in Matlab 2024b by MathWorks (Natick, MA, USA) using the genetic algorithm *ga*. We consider this optimization algorithm since it is able to better analyze the entire space of possible solutions with respect to gradient-base ones. The population size is set equal to 100 for Test A of the seven-DOF robot (two optimization variables), and equal to 150 for Test B of the seven-DOF robot and Test A of the eight-DOF one (four optimization variables). Furthermore, for Test B of the eight-DOF robot (eight optimization variables), a population size equal to 200 is chosen. The numerical tests are performed on a computer running Windows 10 Pro with an Intel Core i9-10900 CPU @ 2.80 GHz and 32.0 GB of RAM.

Table 3. Desired pose of the end-effector of the two considered robotic systems for each of the waypoints of the trajectory in Test B.

Robot	Waypoint	x [m]	y [m]	z [m]	ψ [rad]	ϑ [rad]	φ [rad]
7-DOF robot	1	0.50	0.40	0.30	π	0	$-\pi/4$
	2	0.50	0.40	0.60	$11\pi/12$	$\pi/12$	$-\pi/4$
	3	0.50	-0.40	0.60	$13\pi/12$	$-\pi/12$	$-\pi/4$
	4	0.50	-0.40	0.30	π	0	$-\pi/4$
8-DOF robot	1	0.00	0.50	0.30	π	0	$\pi/4$
	2	0.00	0.50	0.60	$11\pi/12$	$\pi/12$	$\pi/4$
	3	0.80	0.50	0.60	$13\pi/12$	$-\pi/12$	$\pi/4$
	4	0.80	0.50	0.30	π	0	$\pi/4$

Table 4. Joint positions in the homing configurations for the two considered robotic systems.

Robot	q_0 [m]	q_1 [rad]	q_2 [rad]	q_3 [rad]	q_4 [rad]	q_5 [rad]	q_6 [rad]	q_7 [rad]
7-DOF robot	-	0	0	0	$-\pi/2$	0	$\pi/2$	$\pi/4$
8-DOF robot	0.4	$\pi/2$	0	0	$-\pi/2$	0	$\pi/2$	$\pi/4$

4. Numerical Results

4.1. Test A: Point-to-Point Motion

Figures 6 and 7 report the percentage of energy consumption reduction in Test A for the seven-DOF and eight-DOF robots, respectively, compared to the respective reference case. All joints of the seven-DOF robot and all the combinations of joints of the eight-DOF robot are considered as optimization variables. Table 5 shows the energy consumption in Test A with the seven-DOF and eight-DOF robot, for the reference and optimal trajectories. For the seven-DOF robot, the optimal solution is found when the joint q_6^* is considered as an optimization variable, obtaining an energy saving equal to 81.36%. In this case, the energy consumption decreases from 30.23 J to 5.63 J, as it can be seen from Table 5. Considering the eight-DOF robot, the minimum energy consumption is achieved when the position of joints q_3^* and q_5^* is optimized, obtaining a percentage energy consumption reduction of 94.47% (energy expenditure reduction from 98.31 J to 5.44 J, as shown in Table 5). From Table 5, it can be seen that the energy consumption in the optimized case with the eight-DOF robot is lower than the one obtained in the optimal solution with the seven-DOF robot. This result demonstrates that, in this considered case, introducing an additional degree of freedom (and consequently increasing the degree of redundancy) enhances the optimization capabilities of the proposed approach, leading to greater energy savings.

Furthermore, from Figures 6 and 7 it can be noted that most of joints (for the seven-DOF robot) and combinations of two joints (for the eight-DOF robot) to be optimized provide an energy saving close to the optimal solution, demonstrating the capabilities of the proposed approach in minimizing the energy consumption regardless which joint (or combination of joints) position is considered in the optimization problem. In addition to the mechanical energy consumption, Table 5 also reports the joint positions at each considered

waypoint of the Test A for the two considered robotic systems, showing a consistent change in the joint motion in the optimized cases compared to the reference ones. In more detail, in the optimized case for the eight-DOF robotic system, the linear axis is kept stationary during the trajectory. From Table 5, it can be seen that the position of the linear axis (joint q_0) is equal to 0.36 m for both the considered waypoints. In this manner, the linear axis is exploited to optimally position the Panda arm with respect to the task to be executed.

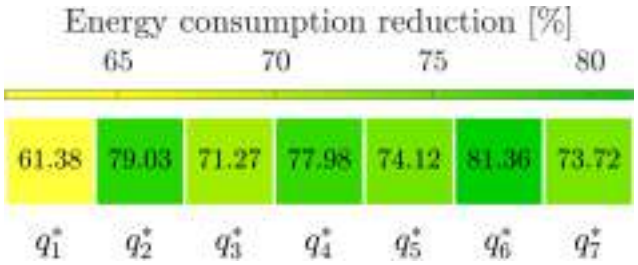

Figure 6. Energy consumption reduction with respect to the reference case in Test A with the 7-DOF robot.

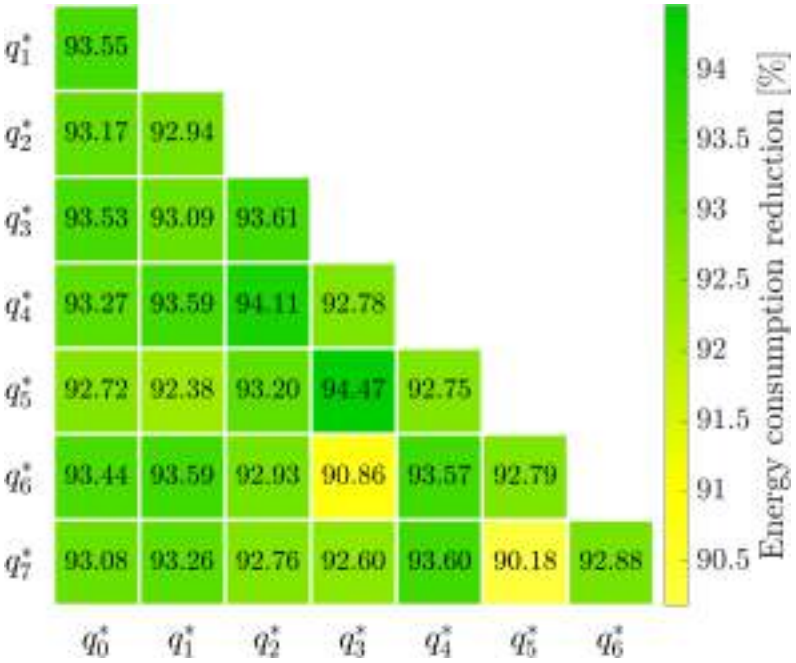

Figure 7. Energy consumption reduction with respect to the reference case in Test A with the 8-DOF robot.

Table 5. Joint positions at each considered waypoint and energy consumed for the reference and optimal trajectories of Test A for the two considered robotic systems.

Robot	Trajectory	Way Point	q_0 [m]	q_1 [rad]	q_2 [rad]	q_3 [rad]	q_4 [rad]	q_5 [rad]	q_6 [rad]	q_7 [rad]	E [J]
7-DOF robot	reference	1	-	0.55	0.76	0.40	−0.76	0.00	1.24	1.64	30.23
		2	-	−0.49	0.45	−0.42	−1.37	0.50	1.99	−0.26	
	optimal (q_6^*)	1	-	1.16	1.18	−1.74	−0.66	1.66	0.84	1.30	5.63
		2	-	0.02	1.18	−1.75	−1.31	1.60	1.40	−0.54	
8-DOF robot	reference	1	0.30	2.01	0.52	0.36	−1.16	0.08	1.37	1.53	98.31
		2	0.50	1.26	0.10	−0.34	−1.84	0.32	2.21	−0.05	
	optimal (q_3^*, q_5^*)	1	0.36	−0.38	−1.18	1.40	−0.70	1.63	0.84	1.28	5.44
		2	0.36	−1.56	−1.18	1.40	−1.29	1.60	1.40	−0.53	

The computational times required to solve the optimization problem in Test A are equal to 2362 s and 2733 s for the seven-DOF and eight-DOF robots, respectively. The computation time depends on several variables, including the degree of redundancy and the number of considered waypoints (i.e., the number of optimization variables). In addition, computational time is influenced by the specific settings of the optimization algorithm. For the genetic algorithm, a larger population size enables a more thorough exploration of the design space and increases the likelihood of obtaining a near-globally optimal solution, at the expense of increased computational time. The proposed approach could be extended to semi-online applications by limiting both the number of iterations of the optimization algorithm and the number of inverse kinematics evaluations, thereby enabling a just-in-time motion planning strategy. This extension could rely on gradient-based optimization methods, which, however, are more prone to convergence to local minima. However, the approach proposed in this work is intended for offline trajectory planning, which is the typical operating mode for the majority of industrial robotic systems, where online motion planning is not required.

4.2. Test B: Pick-and-Place Task

Figures 8 and 9 show the percentage energy consumption reduction in Test B for the seven-DOF and eight-DOF robots, respectively, compared to the respective reference case. For the robot with seven degrees of freedom (Figure 8), each joint q_i^* to be optimized is taken into account in different runs of the optimization problem, whereas all possible combinations of two joints to be optimized are considered in different simulations for the eight-DOF robot (Figure 9). Table 6 reports the energy consumed in Test B with the seven-DOF and eight-DOF robot, for the reference and optimal trajectories. Regarding the seven-DOF manipulator, the lowest energy consumption is obtained when the position of joint q_7^* is considered as optimization variable, achieving an energy saving equal to 26.02%. In this case, the energy expenditure decreases from 76.41 J to 56.52 J, as it can be seen from Table 6. Taking into account the eight-DOF robotic system, the optimal solution is found when the position of joints q_4^* and q_7^* is optimized, leading to a percentage energy consumption reduction of 60.47% (energy expenditure reduction from 124.90 J to 49.38 J, as shown in Table 6). As obtained in Test A, also during Test B, the energy consumption in the optimized case with the eight-DOF robot is lower than the one obtained in the optimal solution with the seven-DOF robot. This outcome highlights again that a greater degree of redundancy could increase the optimization possibilities of the proposed approach, which may result in a lower energy expenditure. In Test B, the computational times are equal to 9466 s and 25,046 s for the seven-DOF and eight-DOF robotic systems, respectively.

Similarly to the results obtained during Test A, also for Test B, an energy saving close to the optimal solution is obtained with most of joints (for the seven-DOF robot) and combinations of two joints (for the eight-DOF robot) to be optimized, as can be seen from Figures 8 and 9. Table 6 shows the joint positions at each considered waypoint of the Test B for the two considered robotic systems. For the tested trajectory, as in the previous case, the optimized solutions show a consistent modification of the joint motions with respect to the reference cases. Additionally, the linear axis is once again maintained fixed throughout the optimal trajectory and exploited to determine the optimal placement of the manipulator with respect to the task.

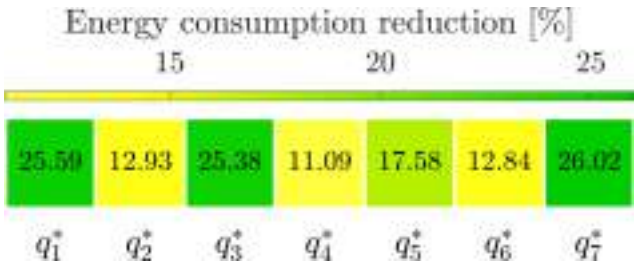

Figure 8. Energy consumption reduction with respect to the reference case in Test B with the 7-DOF robot.

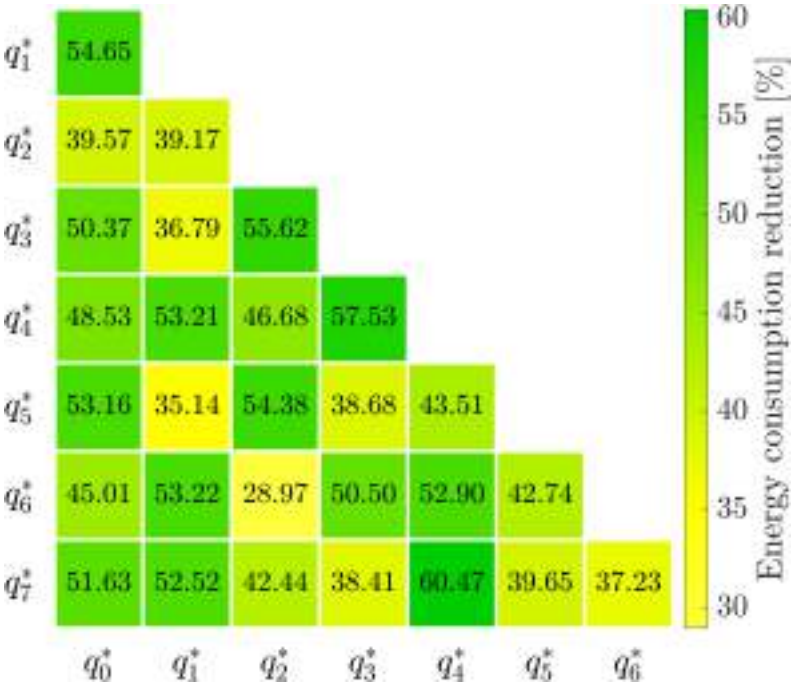

Figure 9. Energy consumption reduction with respect to the reference case in Test B with the 8-DOF robotic system.

Table 6. Joint positions at each considered waypoint and energy consumed for the reference and optimal trajectories of Test B for the two considered robotic systems.

Robot	Trajectory	Way Point	q_0 [m]	q_1 [rad]	q_2 [rad]	q_3 [rad]	q_4 [rad]	q_5 [rad]	q_6 [rad]	q_7 [rad]	E [J]
7-DOF robot	reference	1	-	0.41	0.43	0.29	−1.84	−0.16	2.25	1.56	76.41
		2	-	0.41	0.53	0.39	−0.87	0.06	1.09	1.54	
		3	-	−0.33	0.19	−0.42	−1.48	0.35	1.91	−0.06	
		4	-	−0.41	0.43	−0.29	−1.84	0.16	2.25	0.01	
	optimal (q_7^*)	1	-	1.52	0.67	−0.98	−1.81	0.65	2.12	1.06	56.52
		2	-	1.10	0.67	−0.99	−0.81	0.75	0.95	1.25	
		3	-	0.36	0.67	−1.57	−1.42	1.01	1.62	−0.36	
		4	-	0.17	0.67	−0.98	−1.81	0.65	2.12	−0.29	
8-DOF robot	reference	1	0.31	1.94	0.35	0.25	−1.97	−0.12	2.30	1.47	124.90
		2	0.30	1.89	0.34	0.31	−1.14	0.12	1.17	1.41	
		3	0.47	1.33	−0.04	−0.31	−1.76	0.20	2.03	0.14	
		4	0.46	1.25	0.27	−0.22	−2.08	0.08	2.34	0.19	
	optimal (q_4^*, q_7^*)	1	0.23	0.82	0.92	1.42	−2.05	−1.02	1.97	1.93	49.38
		2	0.23	1.05	0.92	1.80	−1.29	−0.62	1.03	1.86	
		3	0.23	0.19	0.92	1.36	−0.79	−0.76	1.57	0.22	
		4	0.23	0.15	0.92	0.90	−1.35	−0.73	1.93	0.32	

4.3. Comparison with a Null-Space Approach

To compare the efficiency of our reference case with respect to a null-space approach, we use the operational-space trajectories of the reference case as input to the Saturation in the Null Space (SNS) approach presented in [25], which considers joint position and velocity limits as hard constraints in the pseudo-inverse-based solution of the inverse kinematics problem. The results of this comparison are reported in Table 7, which shows that the same trajectory in the operational space of the robot requires a higher energy consumption with the SNS approach, with respect to the proposed reference case, for both Test A and B and for both the considered robotic systems with seven and eight degrees of freedom.

Furthermore, the optimal trajectories obtained with our proposed approach are also used as input to the SNS approach to check the performance of that state-of-the-art redundancy resolution scheme with respect to the results obtained in our work. The comparison results are summarized in Table 7, where it can be seen that the SNS approach shows the worst performance in terms of energy efficiency not only with respect to the baseline, but also to the optimal trajectories considered in this work. This is because, by leaving the path between waypoints free, the optimization problem of the proposed approach has more freedom in solving the robot inverse kinematics problem for energy efficiency than when the end-effector path is completely defined, as required in the SNS approach.

Table 7. Comparison between the energy consumption of the proposed approach and that of the SNS approach computed using the same reference and optimal trajectories.

Test	Robot	Reference Case		Optimal Case	
		Proposed	SNS	Proposed	SNS
A	7-DOF robot	30.23 J	32.35 J	5.63 J	9.38 J
	8-DOF robot	98.31 J	297.35 J	5.44 J	216.98 J
B	7-DOF robot	76.41 J	77.21 J	56.52 J	71.12 J
	8-DOF robot	124.90 J	332.80 J	49.38 J	161.02 J

5. Experimental Tests

The energy-optimal trajectories obtained in the numerical tests are validated on two real robotic systems. In this section, we first describe the experimental setup and the robot control approach, and then we present the results of the experiments.

5.1. Experimental Setup

The seven-DOF Panda arm used in the first test case is shown in Figure 10a and it is available at the Robotics and Mechatronics Lab of University of Udine (Italy). The manipulator is controlled with a computer equipped with 32 GB of RAM and an Intel Core i5 processor running Ubuntu 18.04, using ROS (Robot Operating System) Melodic Morenia with Python 3.6.

The eight-DOF robot is composed of a second Panda arm mounted on a linear axis by AutomationWare (Martellago, Italy). The system is shown in Figure 10b. The linear axis is actuated by an HDT SR08L brushless motor by HDT Srl (Monte di Malo, Italy), connected to the driven pulley of the linear axis through a planetary gearbox with a reduction ratio i_r equal to 10. The cart of the linear axis is moved through a toothed belt made of polyurethane with steel strands.

The eight-DOF robotic system is controlled with a computer equipped with 32 GB RAM and an Intel Core i9 processor running Ubuntu 20.04. As the linear axis and the manipulator are two separated robotic systems, they are driven by two different controllers, which have to be coordinated and synchronized. A schematic representation of the control of the eight-DOF robot is reported in Figure 11. The linear axis is controlled with a Docker container (Docker 1) using ROS 2 Galactic Geochelone, whereas another Docker

container (Docker 2) with ROS Noetic Ninjemys is used for driving the Panda arm, both using Python 3.8. The two Docker containers are able to communicate thanks to a shared network, whereas the *ros1_bridge* package is adopted in order to allow the two different ROS versions to exchange messages. Moreover, the coordination and synchronization of the two robots is performed in the ROS 2 environment (Docker 1), as well as the definition of the desired trajectory that the robotic system has to execute. As can be seen in Figure 11, once the movement of all eight joints has been defined, the trajectory of the different joints is sent to their respective controllers, which will then drive the two distinct components of the system. For both robotic systems, the desired trajectory is sent to the controller as joint positions, velocities, and accelerations over time, whereas the actual joint positions, joint velocities, and torques (motor torque for the linear axis, and joint torques for the manipulator) are acquired as output measured data.

(**a**) (**b**)

Figure 10. Robotic systems considered in this work: 7-DOF robotic manipulator (**a**) and 8-DOF robotic system (**b**).

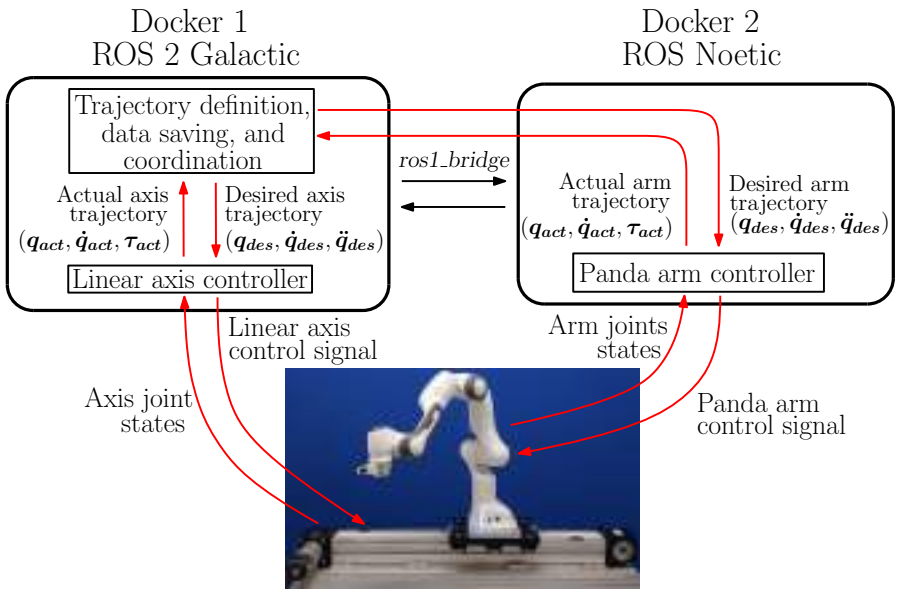

Figure 11. Schematic representation of the control of the 8-DOF robotic system.

5.2. Experimental Results

5.2.1. Test A: Point-to-Point Motion

Table 8 shows and compares the energy consumed in Test A with the two considered robotic systems in the numerical and experimental tests, for the reference and optimal trajectories. As can be seen from Table 8, the energy consumption in the experiments almost coincides with the results obtained in the simulations for all considered trajectories. This

demonstrates the reliability of the dynamics models taken into account for the 7-DOF and 8-DOF robots and the feasibility of the proposed energy-efficiency approach. The actual energy saving achieved in the experiments in Test A with the 7-DOF robot is equal to 82.54% (reduction from 30.29 J to 5.29 J), whereas with the 8-DOF, the percentage of energy reduction with respect to the reference case is equal to 94.28%. In this case, the energy expenditure decreases from 99.22 J to 5.67 J.

Table 8. Energy consumption E for the reference and optimal trajectories of Test A in the numerical (num) and experimental (exp) tests with the two considered robotic systems, and corresponding percentage reductions pct compared to the reference cases.

Robot	Trajectory	E_{num} [J]	pct_{num} [%]	E_{exp} [J]	pct_{exp} [%]
7-DOF robot	reference	30.23	-	30.29	-
	optimal (q_6^*)	5.63	81.36	5.29	82.54
8-DOF robot	reference	98.31	-	99.22	-
	optimal (q_3^*, q_5^*)	5.44	94.47	5.67	94.28

Figure 12 reports the joint positions, velocities, torques, and mechanical powers for the reference (Figure 12a) and optimal (Figure 12b) trajectories with the seven-DOF robot in Test A. Similarly, Figure 13 depicts the joint positions, velocities, torques, and mechanical powers for the reference (Figure 13a) and optimal (Figure 13b) trajectories with the eight-DOF robot in Test A. Comparing Figure 12a with Figure 12b and Figure 13a with Figure 13b, it can be noted the mechanical power is greatly reduced in the optimal cases with respect to the reference ones, leading to the correspondent consistent energy savings reported in Table 8.

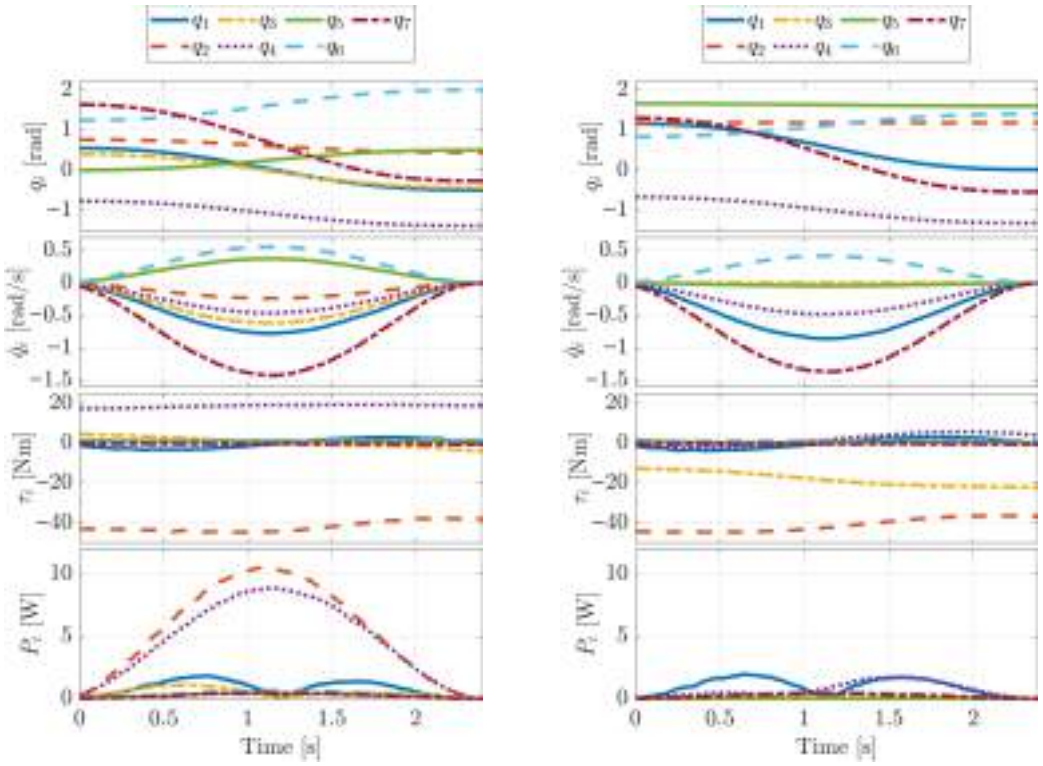

(**a**) Test A, 7-DOF robot, reference trajectory. (**b**) Test A, 7-DOF robot, optimal trajectory.

Figure 12. Joint positions, velocities, torques, and mechanical power of the reference (**a**) and optimal (**b**) trajectories of Test A with the 7-DOF robot.

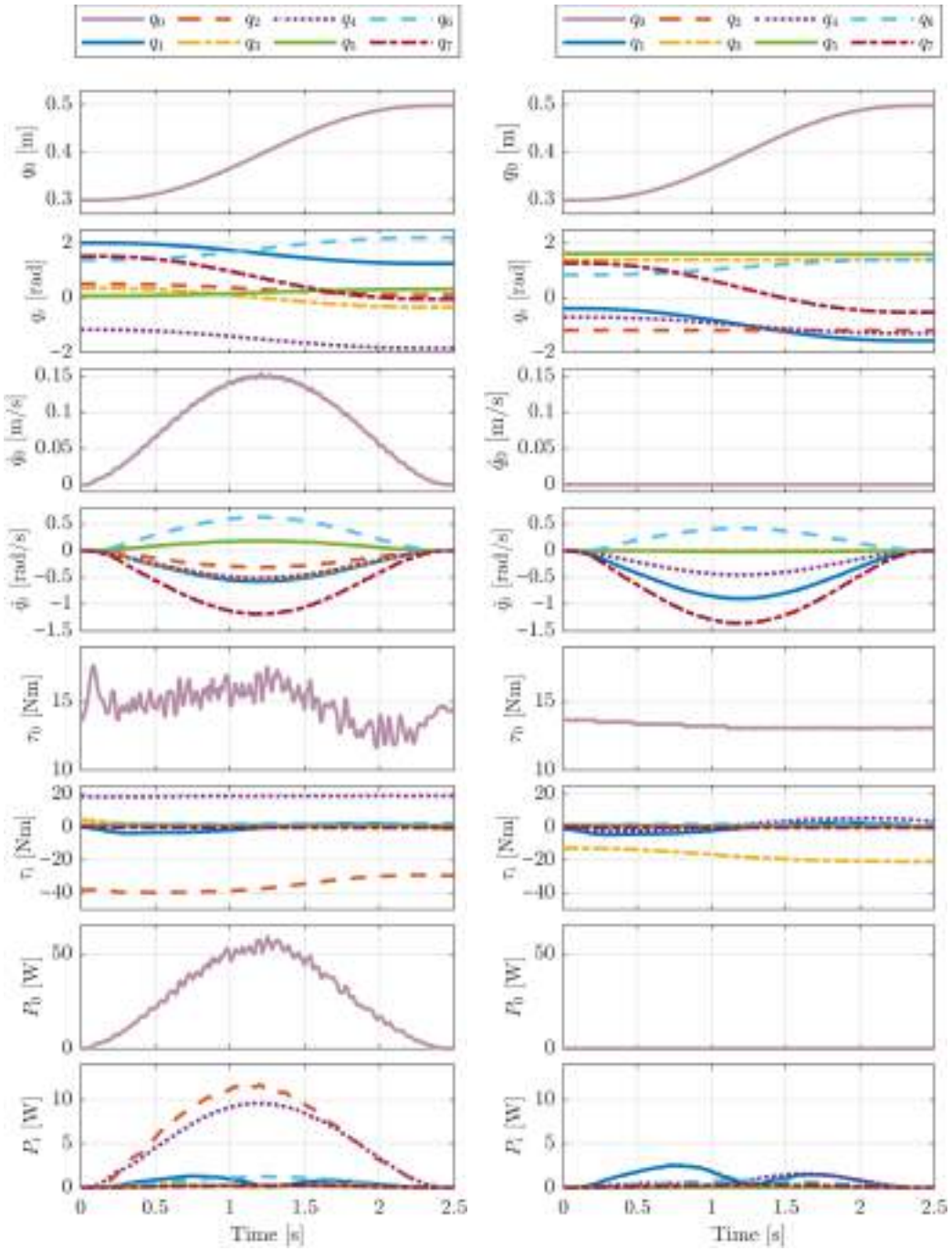

(**a**) Test A, 8-DOF robot, reference trajectory. (**b**) Test A, 8-DOF robot, optimal trajectory.

Figure 13. Joint positions, velocities, torques, and mechanical power of the reference (**a**) and optimal (**b**) trajectories of Test A with the 8-DOF robot.

5.2.2. Test B: Pick-and-Place Task

In Table 9, the energy consumed with the two considered robotic systems in Test B during the numerical and experimental tests is reported, both for the reference and the optimal trajectories. Similarly to Test A, Table 9 highlights that the energy consumption in Test B during the experiments is very close to those obtained in the simulations for all considered trajectories, proving again the feasibility of the proposed energy-efficiency approach. With the seven-DOF robot, the energy consumption in the experiments in Test B is reduced from 75.62 J (reference case) to 55.68 J (optimal trajectory), obtaining a percentage of energy reduction equal to 26.37%. Considering the eight-DOF robot, the percentage of

energy reduction with respect to the reference case is equal to 60.14%, achieving a decrease in the energy expenditure from 123.75 J to 49.33 J.

Table 9. Energy consumption E for the reference and optimal trajectories of Test B in the numerical (num) and experimental (exp) tests with the two considered robotic systems, and corresponding percentage reductions pct compared to the reference cases.

Robot	Trajectory	E_{num} [J]	pct_{num} [%]	E_{exp} [J]	pct_{exp} [%]
7-DOF robot	reference	76.41	-	75.62	-
	optimal (q_7^*)	56.52	26.02	55.68	26.37
8-DOF robot	reference	124.90	-	123.75	-
	optimal (q_4^*, q_7^*)	49.38	60.47	49.33	60.14

Figure 14 shows the joint positions, velocities, torques, and mechanical powers for the reference (Figure 14a) and optimal (Figure 14b) trajectories with the seven-DOF robot in Test B, whereas Figure 15 reports the same graphs for the eight-DOF robot in Test B. As for Test A, the comparisons of Figure 14a with Figure 14b as well as Figure 15a with Figure 15b highlight the significant reduction in mechanical power needed by the optimal trajectories with respect to the reference ones.

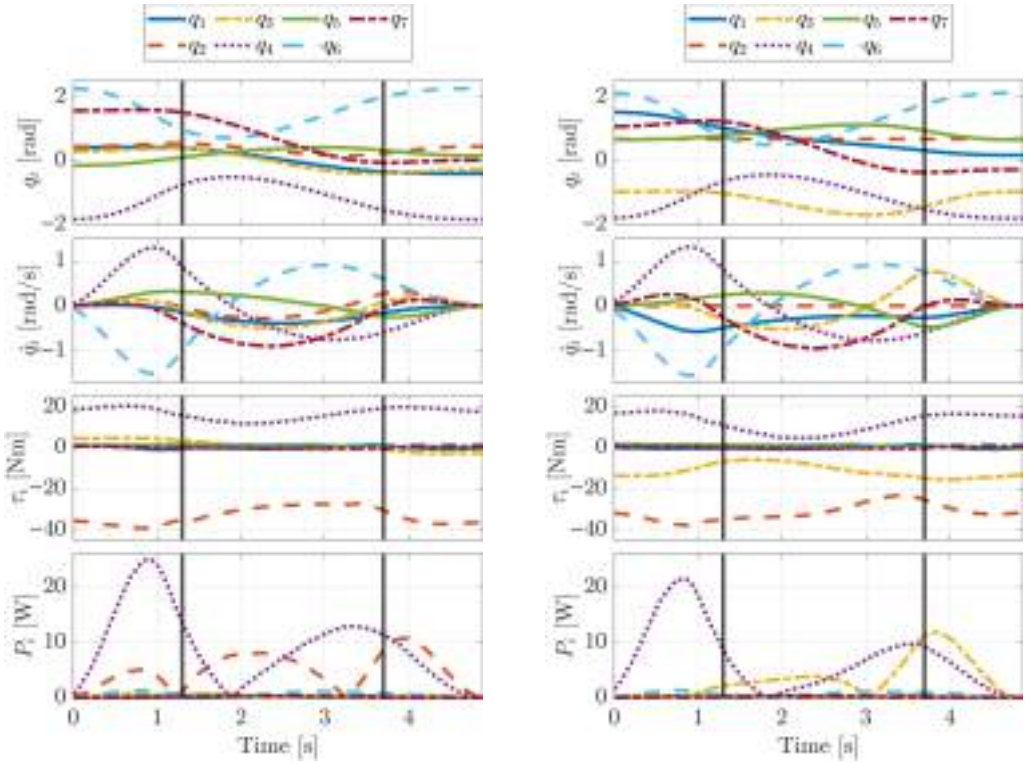

(**a**) Test B, 7-DOF robot, reference trajectory. (**b**) Test B, 7-DOF robot, optimal trajectory.

Figure 14. Joint positions, velocities, torques, and mechanical power of the reference (**a**) and optimal (**b**) trajectories of Test B with the 7-DOF robot.

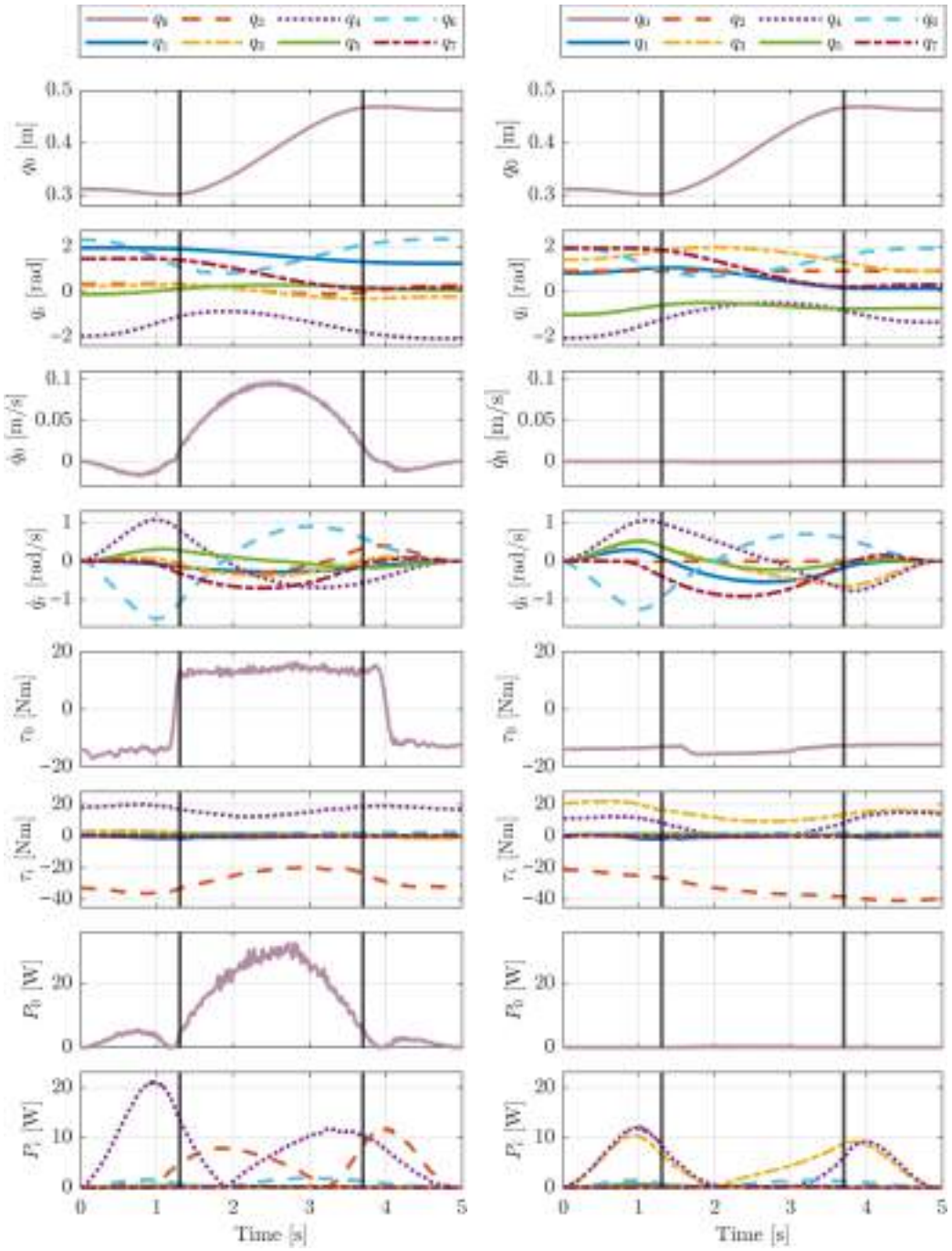

(**a**) Test B, 8-DOF robot, reference trajectory. (**b**) Test B, 8-DOF robot, optimal trajectory.

Figure 15. Joint positions, velocities, torques, and mechanical power of the reference (**a**) and optimal (**b**) trajectories of Test B with the 8-DOF robot.

6. Conclusions

In this paper, an energy-efficiency approach for redundant robotic systems has been presented. The proposed strategy aims at finding the energy-optimal solution of the inverse kinematics by optimizing the position of selected redundant joints at each of the waypoints that describe a pre-defined task. The performance of proposed approach has been tested on a seven-DOF robotic manipulator and on a eight-DOF robotic system, so as to account for different degrees of redundancy. As test cases, a point-to-point motion and a pick-and-place task have been selected, performing extensive numerical simulations and experimental tests. The numerical and experimental results highlighted the capabilities of the proposed

approach in improving the energetic performance with respect to reference trajectories. The experimental results showed a reduction in the energy expenditure up to 82.54% and 94.28% with the 7-DOF and the 8-DOF robots, respectively.

Future work will include the development and investigation of alternative and more complex redundancy resolution and motion planning strategies for energy efficiency purposes. The results obtained will then be compared with those of this work. Furthermore, artificial-intelligence-based methods for computing minimum-energy solutions of the inverse kinematics problem will be considered.

Author Contributions: Conceptualization, methodology, L.S.; software, validation, formal analysis, G.F.; investigation, data curation, G.F. and L.S.; writing—original draft preparation, G.F.; writing—review and editing, G.F., L.S. and A.G.; supervision, project administration, funding acquisition, L.S. and A.G. All authors have read and agreed to the published version of the manuscript.

Funding: This work has been supported by iNEST-Interconnected NordEst Innovation Ecosystem, funded by PNRR (Mission 4.2, Investment 1.5), NextGeneration EU—Project ID: ECS 00000043, and developed within the Laboratory for Big Data, IoT, Cyber Security (LABIC) funded by Friuli Venezia Giulia region (Italy), and the Laboratory for Artificial Intelligence for Human-Robot Collaboration (AI4HRC) funded by Fondazione Friuli (Italy).

Institutional Review Board Statement: Not applicable.

Informed Consent Statement: Not applicable.

Data Availability Statement: Data will be made available upon request.

Conflicts of Interest: The authors declare no conflicts of interest.

References

1. De Simone, V.; Di Pasquale, V.; Giubileo, V.; Miranda, S. Human-Robot Collaboration: An analysis of worker's performance. *Procedia Comput. Sci.* **2022**, *200*, 1540–1549. [CrossRef]
2. Jiang, P.; Wang, Z.; Li, X.; Wang, X.V.; Yang, B.; Zheng, J. Energy consumption prediction and optimization of industrial robots based on LSTM. *J. Manuf. Syst.* **2023**, *70*, 137–148. [CrossRef]
3. Clochiatti, E.; Scalera, L.; Boscariol, P.; Gasparetto, A. Electro-mechanical modeling and identification of the UR5 e-series robot. *Robotica* **2024**, *42*, 2430–2452.
4. Yang, D.; Wei, X.; Han, M. Research on Energy Consumption Optimization Strategies of Robot Joints Based on NSGA-II and Energy Consumption Mapping. *Robotics* **2025**, *14*, 138. [CrossRef]
5. The Sustainable Development Goals of the United Nations. Available online: https://sdgs.un.org/goals (accessed on 10 January 2026).
6. Bugday, M.; Karali, M. Design optimization of industrial robot arm to minimize redundant weight. *Eng. Sci. Technol. Int. J.* **2019**, *22*, 346–352. [CrossRef]
7. Khalaf, P.; Richter, H. Trajectory optimization of robots with regenerative drive systems: Numerical and experimental results. *IEEE Trans. Robot.* **2019**, *36*, 501–516. [CrossRef]
8. Althoff, M.; Giusti, A.; Liu, S.B.; Pereira, A. Effortless creation of safe robots from modules through self-programming and self-verification. *Sci. Robot.* **2019**, *4*, eaaw1924. [CrossRef] [PubMed]
9. Vivas, A.V.; Cherubini, A.; Garabini, M.; Salaris, P.; Bicchi, A. Minimizing energy consumption of elastic robots in repetitive tasks. *IEEE Trans. Syst. Man Cybern. Syst.* **2023**, *53*, 5006–5018. [CrossRef]
10. Bruzzone, L.; Verotti, M.; Fanghella, P. A Comparative Study of Natural and Exact Elastic Balancing Methods for the RR-4R-R Manipulator. *Machines* **2025**, *13*, 1023. [CrossRef]
11. Ruzarovsky, R.; Horak, T.; Bocak, R. Evaluating Energy Efficiency and Optimal Positioning of Industrial Robots in Sustainable Manufacturing. *J. Manuf. Mater. Process.* **2024**, *8*, 276. [CrossRef]
12. Fabris, G.; Scalera, L.; Gasparetto, A. Dynamic modelling and energy-efficiency optimization in a 3-DOF parallel robot. *Int. J. Adv. Manuf. Technol.* **2024**, *132*, 2677–2699. [CrossRef]
13. Li, X.; Lan, Y.; Jiang, P.; Cao, H.; Zhou, J. An efficient computation for energy optimization of robot trajectory. *IEEE Trans. Ind. Electron.* **2021**, *69*, 11436–11446. [CrossRef]

14. Fabris, G.; Scalera, L.; Gasparetto, A. Online optimization of minimum-time and minimum-energy trajectories for a 1-DOF belt-driven robotic system. *Robotica* **2025**, *43*, 2030–2045. [CrossRef]
15. De Laet, R.; Van Oosterwyck, N.; Scalera, L.; Cuyt, A.; Gasparetto, A.; Derammelaere, S. Energy-efficient motion planning for robotic systems using polynomials in the Chebyshev basis. *Robot. Auton. Syst.* **2025**, *192*, 105051. [CrossRef]
16. Elgohr, A.T.; Khater, H.A.; Mousa, M.A. Trajectory optimization for 6 DOF robotic arm using WOA, GA, and novel WGA techniques. *Results Eng.* **2025**, *25*, 104511. [CrossRef]
17. Wang, X.; Cao, J.; Cao, Y.; Zou, F. Energy-efficient trajectory planning for a class of industrial robots using parallel deep reinforcement learning. *Nonlinear Dyn.* **2025**, *113*, 8491–8511.
18. Sciavicco, L.; Siciliano, B. *Modelling and Control of Robot Manipulators*; Springer Science & Business Media: London, UK, 2012.
19. Fabregat-Jaén, M.; Peidró, A.; Colombo, M.; Rocco, P.; Reinoso, Ó. Topological and spatial analysis of self-motion manifolds for global redundancy resolution in kinematically redundant robots. *Mech. Mach. Theory* **2025**, *210*, 106020. [CrossRef]
20. Monari, E.; Chen, Y.; Vertechy, R. On locally optimal redundancy resolution using the basis of the null space. In *Proceedings of the 2023 IEEE International Conference on Robotics and Automation (ICRA)*; IEEE: New York, NY, USA, 2023; pp. 9665–9671.
21. Hong, T.; Li, W.; Huang, K. A reinforcement learning enhanced pseudo-inverse approach to self-collision avoidance of redundant robots. *Front. Neurorobot.* **2024**, *18*, 1375309.
22. Shahabi, M.; Ghariblu, H. Optimal joint motion for complicated welding geometry by a redundant robotic system. *Eng. Optim.* **2020**, *52*, 875–895. [CrossRef]
23. Vu, M.N.; Beck, F.; Schwegel, M.; Hartl-Nesic, C.; Nguyen, A.; Kugi, A. Machine learning-based framework for optimally solving the analytical inverse kinematics for redundant manipulators. *Mechatronics* **2023**, *91*, 102970. [CrossRef]
24. Nguyen, L.A.; Le, K.D.; Harman, T.L. Kinematic redundancy resolution for Baxter robot. In *Proceedings of the 2021 7th International Conference on Automation, Robotics and Applications (ICARA)*; IEEE: New York, NY, USA, 2021; pp. 6–9.
25. Flacco, F.; De Luca, A.; Khatib, O. Motion control of redundant robots under joint constraints: Saturation in the Null Space. In *Proceedings of the 2012 IEEE International Conference on Robotics and Automation (ICRA)*; IEEE: New York, NY, USA, 2012; pp. 285–292.
26. Fiore, M.D.; Meli, G.; Ziese, A.; Siciliano, B.; Natale, C. A general framework for hierarchical redundancy resolution under arbitrary constraints. *IEEE Trans. Robot.* **2023**, *39*, 2468–2487. [CrossRef]
27. Doan, N.C.N.; Tao, P.Y.; Lin, W. Optimal redundancy resolution for robotic arc welding using modified particle swarm optimization. In *Proceedings of the 2016 IEEE International Conference on Advanced Intelligent Mechatronics (AIM)*; IEEE: New York, NY, USA, 2016; pp. 554–559.
28. Ruiz, A.G.; Santos, J.C.; Croes, J.; Desmet, W.; da Silva, M.M. On redundancy resolution and energy consumption of kinematically redundant planar parallel manipulators. *Robotica* **2018**, *36*, 809–821. [CrossRef]
29. Sutjipto, S.; Woolfrey, J.; Carmichael, M.G.; Paul, G. Cartesian Inertia Optimization via Redundancy Resolution for Physical Human-Robot Interaction. In *Proceedings of the 2021 IEEE 17th International Conference on Automation Science and Engineering (CASE)*; IEEE: New York, NY, USA, 2021; pp. 570–575.
30. Li, X.; Liu, H.; Dong, M. A general framework of motion planning for redundant robot manipulator based on deep reinforcement learning. *IEEE Trans. Ind. Inform.* **2021**, *18*, 5253–5263. [CrossRef]
31. Fabris, G.; Scalera, L.; Gasparetto, A. Leveraging Kinematic Redundancy for Energy Efficiency in a 8-DOF Robotic System. In *Mechanisms and Machine Science, Proceedings of I4SDG Workshop 2025—IFToMM for Sustainable Development Goals. I4SDG 2025*; Carbone, G., Quaglia, G., Eds.; Springer: Cham, Switzerland, 2025; Volume 179, pp. 340–348.
32. Gaz, C.; Cognetti, M.; Oliva, A.; Giordano, P.R.; De Luca, A. Dynamic identification of the Franka Emika Panda robot with retrieval of feasible parameters using penalty-based optimization. *IEEE Robot. Autom. Lett.* **2019**, *4*, 4147–4154. [CrossRef]